Bragg Soliton Compression and Fission on CMOS-Compatible Ultra-Silicon-Rich Nitride

Ezgi Sahin, Andrea Blanco-Redondo, Peng Xing, Doris K. T. Ng, Ching E. Png, Dawn T. H. Tan,* and Benjamin J. Eggleton**

Higher-order soliton dynamics, specifically soliton compression and fission, underpin crucial applications in ultrafast optics, communications, and signal processing. Bragg solitons exploit the strong dispersive properties of periodic media near the photonic band edge. This enables soliton dynamics to occur in very short propagation distances, opening avenues to harness soliton compression and fission in integrated photonic platforms. However, implementation in complementary metal-oxide semiconductor (CMOS)-compatible platforms has been hindered by the strong nonlinear loss that dominates the propagation in silicon and the low-optical nonlinearity of traditional silicon nitride. Here, CMOS-compatible, on-chip Bragg solitons, are presented with a soliton-effect pulse compression with a factor of × 5.7, along with time-resolved measurements of soliton fission on a CMOS-compatible photonic circuit platform. These observations are enabled by the combination of a unique cladding-modulated Bragg grating design and the high nonlinearity and negligible nonlinear loss of compositionally engineered ultra-silicon-rich nitride (USRN: Si_7N_3).

1. Introduction

Temporal optical solitons, first demonstrated by Mollenauer et al.[1] in optical fiber, were explored for their use in fiber communications to transmit information as they preserve their shape during propagation.[2–4] This dispersionless propagation of the fundamental soliton is due to the balance between self-phase modulation (SPM) and group velocity dispersion (GVD) in the fiber media. Since then, harnessing soliton dynamics has enabled numerous applications and underpins many contemporary nonlinear optical systems, such as pulse compression,[5–9] pulse train generation,[10–12] supercontinuum (SC) generation,[13–16] and stable frequency comb generation.[17,18]

Whereas fundamental solitons preserve their shape during propagation, high-order solitons evolve periodically due to the interplay of linear dispersion and Kerr effects in the material. This periodic evolution involves temporal compression, pulse splitting, and recovery of the initial soliton pulse shape. A strong perturbation in the system can break this periodicity, and initiate soliton fission,[19–21] which manifests as pulse breakup and pulse train generation; under certain conditions, this can also be described in terms of modulational instability. [11] This nonlinear optical effect, which is also one of the underlying physical effects involved in SC generation,[13] introduces pulse modulations in time, compression, and splitting, giving rise to spectral broadening and new peaks in the spectrum.

In 1987, Chen and Mills theoretically predicted a new class of optical soliton, associated with the Kerr nonlinearity of the material and the strong dispersion induced at frequencies close to the edge of the stop-band of a periodic structure (e.g., a Bragg grating).[22] These so-called gap solitons[22–25] propagate at frequencies within the stop-band induced by the periodic structure, where the transmission is low, and exploit the intensity-dependent refractive index to switch the stop-band from reflection to transmission dynamically. The more general class of optical soliton in one-dimensional periodic structures is referred to as Bragg solitons,[6,26] in which case the propagation frequencies can lie outside of the stop-band, close to the blue edge where the dispersion is anomalous, and the grating transmission can be high, particularly if it is apodized. Bragg soliton propagation

E. Sahin, P. Xing, Prof. D. T. H. Tan
Photonics Devices and Systems Group
Singapore University of Technology and Design
8 Somapah Rd., Singapore 487372, Singapore
E-mail: ezgi_sahin@mymail.sutd.edu.sg; dawn_tan@sutd.edu.sg

E. Sahin, Dr. C. E. Png
Electronics and Photonics Department
Institute of High Performance Computing
Agency for Science, Technology and Research, 1 Fusionopolis Way, Singapore 138632, Singapore

Dr. A. Blanco-Redondo, Prof. B. J. Eggleton
Institute of Photonics and Optical Science
School of Physics
The University of Sydney
New South Wales 2006, Australia
E-mail: benjamin.eggleton@sydney.edu.au

Dr. A. Blanco-Redondo, Prof. B. J. Eggleton
The University of Sydney Nano Institute
The University of Sydney
New South Wales 2006, Australia

Dr. D. K. T. Ng
Institute of Microelectronics
A*STAR, 2 Fusionopolis Way, #08-02, Innovis Tower, Singapore 138634, Singapore

The ORCID identification number(s) for the author(s) of this article can be found under https://doi.org/10.1002/lpor.201900114

DOI: 10.1002/lpor.201900114

© 2019 WILEY-VCH Verlag GmbH & Co. KGaA, Weinheim

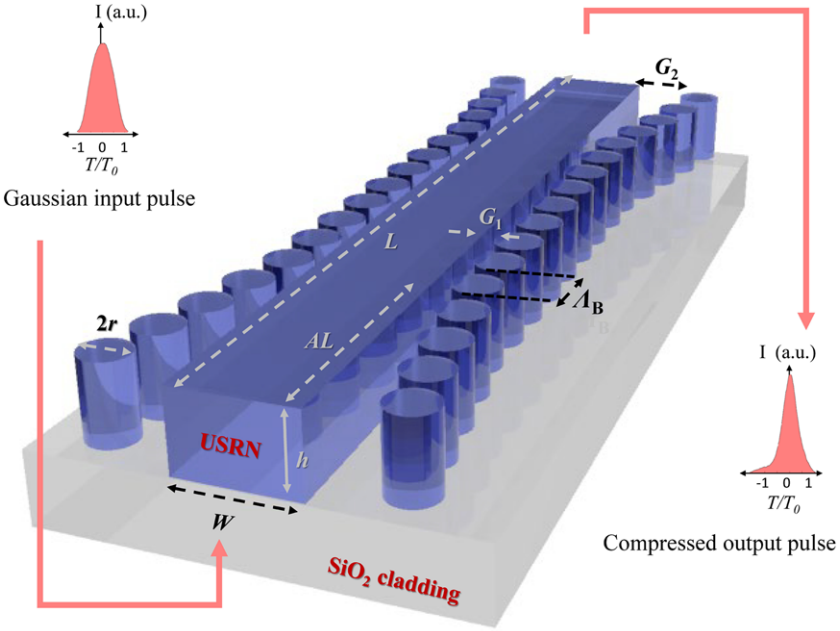

Figure 1. 3D schematic of cladding-modulated Bragg gratings (CMBGs) showing its apodization length (*AL*) with parameters denoted: pitch (Λ_B), waveguide width (*W*), height (*h*), length (*L*) and pillar radius (*r*) and gaps (G_1 & G_2). Input and output pulses show the effect of nonlinear pulse propagation along a Bragg grating at wavelengths close to the stop-band for a picosecond pulse.

in fiber-based periodic structures has been studied extensively, and is the basis of a range of soliton dynamics, such as pulse compression via higher-order soliton evolution and pulse-train generation via modulational instability or soliton fission.[6,10,11,27] The strong band-edge dispersion allows for soliton dynamics to be studied and harnessed on significantly shorter lengths scales; experiments to date have been reported in centimeter scale holographically written optical fiber Bragg gratings.[11,24]

However, implementation of Bragg solitons on a chip has been hindered by design and fabrication challenges. The periodicity that induces the strong band-edge dispersion brings about practical difficulties such as stitching errors[28] and sidewall roughness[29] in on-chip fabrication processes. These fabrication inaccuracies in periodic structures give rise to phase discontinuities that can compromise the dispersive properties of the grating band edge, thus precluding their usefulness.[30] In particular, sidewall corrugated Bragg gratings are prone to distortions in spectral response due to waveguide dimension fluctuations. Cladding modulated Bragg gratings (CMBG), are one of the schemes[31–34] that aim to overcome these difficulties, enabling high-quality apodized Bragg gratings. Details on CMBG was presented previously.[34,35] Material challenges in complementary metal-oxide semiconductor (CMOS) platforms have also impeded progress: Silicon waveguides possess non-negligible nonlinear losses at near-infrared wavelengths, and traditional silicon nitride has low optical nonlinearity.

In this paper, we report the observation of Bragg solitons and associated dynamics in a CMOS-compatible integrated device, observing Bragg soliton-induced compression up to a factor of × 5.7. This large soliton-effect compression factor (on a CMOS-compatible platform) and observation of soliton fission are enabled by the large Kerr nonlinearity and absence of nonlinear losses intrinsic to the ultra-silicon-rich nitride platform, and the large GVD induced by the periodicity in the integrated cladding-modulated apodized Bragg grating. We present time-resolved measurements of soliton fission on a CMOS-compatible platform using frequency-resolved electrical gating (FREG), which allows us to acquire the exact temporal shape and phase information of the output ultrashort pulses. We confirmed our results and elucidated the underlying physics with numerical modeling via the generalized nonlinear Schrödinger equation (GNLSE).

2. Material Platform and the Cladding-Modulated Bragg Gratings

We created the ultra-silicon-rich nitride[16,36] platform with a material composition of Si_7N_3 to overcome the nonlinear loss limitations found in silicon at the prolific 1.55 µm wavelength region[37,38] while retaining a large nonlinearity. USRN is a CMOS-compatible platform that unlocks an order of magnitude larger Kerr nonlinearity ($n_2 = 2.8 \times 10^{-13}$ cm^{2}W^{-1}) compared to stoichiometric silicon nitride in the absence of nonlinear losses. This is made possible via engineering the material's silicon and nitrogen composition to achieve a sufficiently large bandgap to eliminate two-photon absorption. SC generation[16] and high-gain optical parametric amplification[36] were previously demonstrated on this platform and details on fabrication can be found in Supporting Information.

Experimental time-resolved characterization of Bragg soliton dynamics is performed on CMBGs.[34,35] The 3D schematic of our device which has silica under- and over-cladding is given in **Figure 1**. These structures allow dispersion engineering

© 2019 WILEY-VCH Verlag GmbH & Co. KGaA, Weinheim

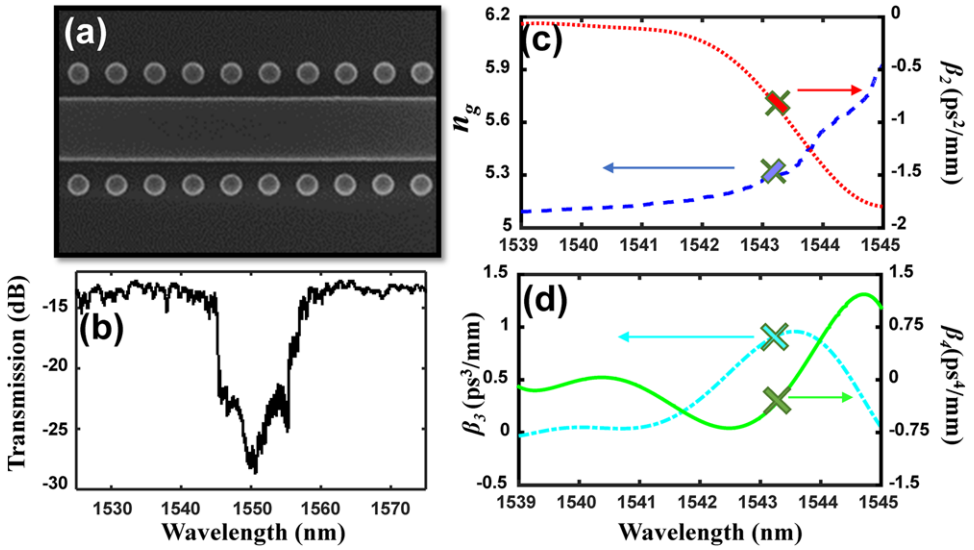

Figure 2. Scanning electron microscopy (SEM) image and optical properties of the CMBG. a) SEM image taken before cladding deposition. b) Transmission of CMBG showing the bandgap of 10 nm. c) Group index (n_g) and group velocity dispersion (β_2). d) Third-order (β_3) and fourth-order (β_4) dispersion curves.

by providing wide flexibility for achieving complex gratings via their tunable parameters such as pillar radius (r), gap (G), and grating pitch (Λ_B). Details on CMBG parameters can be found in Supporting Information. Compared to PhCWgs which are largely implemented using membrane structures, CMBGs require a simple lithographic step with no sacrificial etch and are thus more structurally robust. Compared to Bragg gratings that exploit photosensitivity (e.g., photodarkening), these structures are more stable. The unique cladding-modulated grating design allows for effective apodization in the input and output ends of the grating to minimize sidelobes and ensure low insertion loss at frequencies close the stop-band.[35]

Apodization can be easily understood through the schematic shown in Figure 1. The apodization profile is implemented by continuously decreasing the pillar-waveguide gap from $G_2 = 150$ nm to $G_1 = 50$ nm over apodization length $AL = 600$ µm according to a raised cosine function

$$G(z) = (G_2 - G_1) \times \cos^2(\pi x) + G_1$$
$$\text{where } x = \begin{cases} \dfrac{z}{2AL} & \text{if } z \le AL \\ 0.5 & \text{if } AL < z < L - AL \\ \dfrac{z - L}{2AL} & \text{if } z \ge L - AL \end{cases} \quad (1)$$

This modulation of the distance between the pillars and the waveguide changes the effective refractive index (n_{eff}) perturbation. Avoiding an abrupt change in n_{eff} eliminates the out of band ripples as the apodization suppresses the grating sidelobes without influencing the Bragg wavelength ($\lambda_B = 2n_{eff}\,\Lambda_B$). We fabricated a CMBG of total grating length $L = 6$ mm with pitch, $\Lambda_B = 339$ nm. Considering the apodization length of 600 µm, the grating section with a constant pillar-waveguide gap possesses a length, $L_g = L - 2AL = 4.8$ mm. A scanning electron micrograph of the fabricated device before the deposition of the SiO_2 cladding is shown in **Figure 2**a.

The linear transmission of our grating was first measured using an amplified spontaneous emission source and an inline polarizer to ensure transverse-electric polarization. An optical spectrum analyzer was used to measure the grating's transmission spectrum. Figure 2b shows the transmission spectrum of our CMBG with its bandgap centered close to 1.55 µm. We measured the group index n_g with a component analyzer that uses an interferometric technique. The dispersion parameters are derived from the polynomial fitting of the group index curve shown in Figure 2c. The GVD, (β_2), third-order dispersion (TOD, β_3) and fourth-order dispersion (FOD, β_4) curves are shown in Figure 2c,d. The grating dispersion parameters are extracted to be, $\beta_2 = -0.81$ ps^2 mm^{-1}, $\beta_3 = 0.83$ ps^3 mm^{-1}, $\beta_4 = -0.33$ ps^4 mm^{-1}. Dispersion lengths are given by $L_{Dx} = \frac{T_0^x}{\beta_x}$, where x denotes the order of dispersion. We used the experimentally obtained values of β_n to calculate the corresponding dispersion lengths as $L_{D2} = 10.8$ mm, $L_{D3} = 31.3$ mm, and $L_{D4} = 23.3$ cm at $\lambda = 1543.1$ nm, considering a pulse full-width half-maximum (FWHM) of 4.93 ps ($T_{FWHM} \approx 1.665 \times T_0$). L_{D2} and L_{D3} are sufficiently small that GVD and TOD will have a significant effect on the nonlinear pulse propagation dynamics whereas FOD may be assumed to be of minor importance.

3. High-Order Soliton Dynamics in USRN Gratings

Soliton propagation in USRN can be modeled by solving the GNLSE which is a good approximation in this regime[39–41] via the split-step Fourier method

$$\frac{\partial A}{\partial z} = -\frac{\alpha}{2}A + i\sum_{k=2}^{6}\frac{i^k}{k!}\beta_k\frac{\partial^k A}{\partial T^k} + i\gamma_{eff}\left(|A|^2 A\right) \quad (2)$$

© 2019 WILEY-VCH Verlag GmbH & Co. KGaA, Weinheim

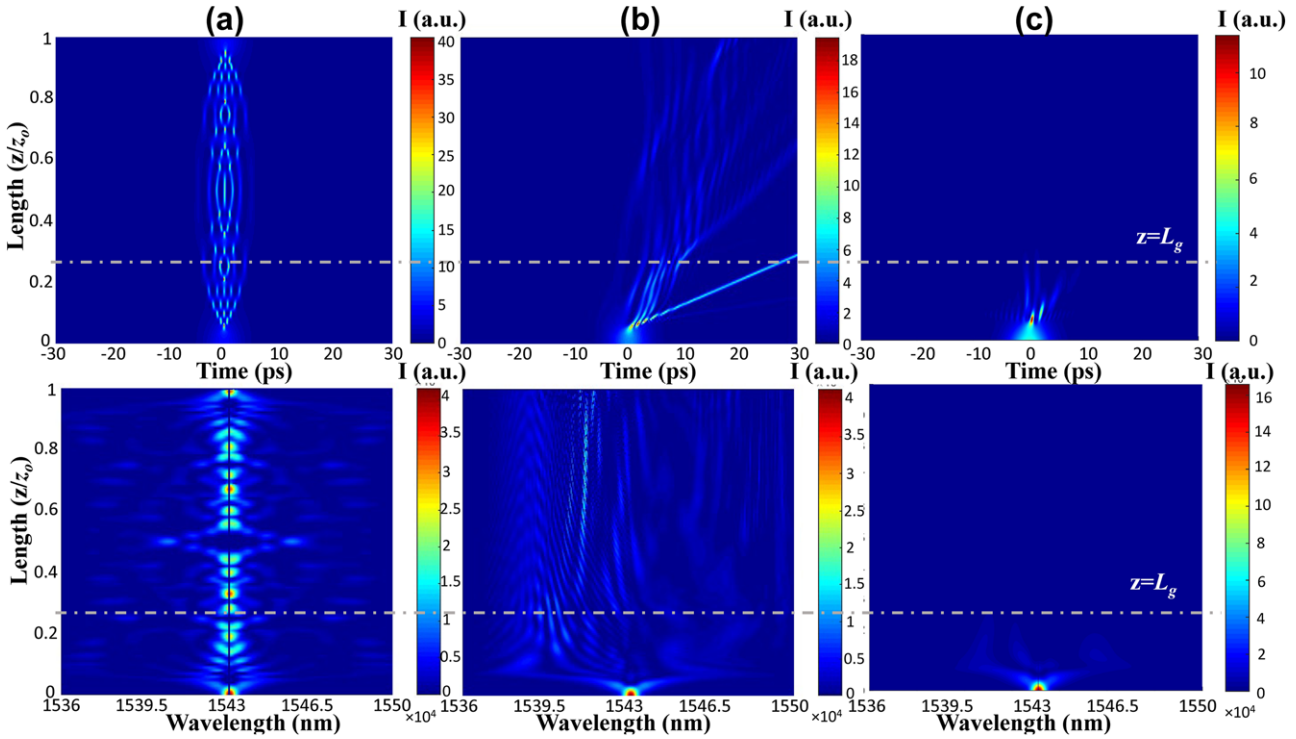

Figure 3. Modeled temporal and spectral intensity plots showing the pulse evolution along one soliton period for the soliton order $N = 8$. The uniform grating length, L_g is marked on the plots. a) Pulse evolution where only GVD and SPM effects are present. b) Soliton fission after initial pulse compression when TOD effects are included in the modeling. c) Including all the effects given in Equation (2).

The GNLSE assumes that the pulse envelope denoted by $A(z,t)$ is slowly varying. Contributions of chromatic dispersion to the pulse propagation dynamics is included through the second term at the right-hand side. The last term of Equation (2) takes self-phase modulation (SPM) into account. γ_{eff} denotes the effective nonlinear parameter and is calculated as $\gamma_{\text{eff}} = \frac{\omega_0}{c}\frac{n_2}{A_{\text{eff}}}\left(\frac{n_g}{n_o}\right)^2$, where ω_0 is the frequency of the pulse, n_g is the group index, and n_o is the refractive index of the material. The effective area (A_{eff}) is engineered to be small in order to maximize the magnitude of γ_{eff}. Nonlinear losses have been shown to be negligible at optical intensities up to 50 GW cm^{-2} for the USRN platform,[16] significantly larger than the power levels used in this experiment. Therefore, we only take the linear propagation losses, α, into account.

It has been well established that the GNLSE is a good approximation to the nonlinear coupled mode equations for describing soliton pulse dynamics in Bragg gratings for frequencies outside of the stop-band within limits described below. De Sterke et al. showed, that this approximation is valid where the frequency of operation is close to the upper edge of the gap, and not in the middle of the photonic bandgap.[41] Eggleton et al. later established two constraints for the validity of NLSE in modeling Bragg soliton propagation.[42] The first constraint is on the field bandwidth, requiring $c\kappa\tau \gg 1$. The grating used here has a coupling coefficient $\kappa = 68$ mm^{-1}, giving us $c\kappa\tau = 102$. We believe that two orders of magnitude is sufficiently large to use the approximation in Equation (2). The second constraint is on the light intensity: $n_2 I << \Delta n$. The calculated value of refractive index perturbation, Δn, in this manuscript for $G = 50$ nm is 0.058. The maximum $n_2 I$ is calculated to be 6.41×10^{-4}. Therefore, $n_2 I$ is 90 × smaller than Δn, satisfying the condition, $n_2 I << \Delta n$.

Higher-order solitons are bound states of fundamental solitons that undergo recurrent periodic propagation. The soliton order N is defined as, $N^2 = \frac{L_D}{L_{NL}} = \frac{T_0^2 \gamma_{\text{eff}} P_0}{|\beta_2|}$ where P_0 refers to the peak power. In the absence of perturbative effects (i.e., TOD, free-carrier (FC), and two-photon absorption (TPA)), an $N = 1$ soliton propagating through the waveguide preserves its shape over the propagation length; this corresponds to a fundamental soliton. Higher-order solitons exhibit more complex temporal dynamics; they periodically compress, split into multiple pulses, and recover their original shape. When N is an integer number, this periodic evolution occurs at exactly one soliton period, $z_0 = \pi/2 \times L_{D2}$.[3] When TOD effects are sufficiently large, the delicate balance of GVD and SPM is disrupted, and this symmetric and periodic soliton evolution ceases to exist. In the absence of TOD, the fundamental solitons comprising a higher-order soliton are bound and behave as a breather, as all of them propagate at the same speed. The presence of TOD breaks that degeneracy and causes the separation of higher-order soliton into its constituents. These separated solitons then travel further apart from each other in the guiding media rather than evolving back into their initial pulse shape at $z = z_0$.

To reveal the underlying physics in the propagation of high-order solitons and their fission, we examine the "ideal" pulse evolution in the gratings where $N = 8$ and only SPM and GVD effects are present. As expected, the interplay of the dispersion and nonlinearity results in a complex periodic evolution of the breathers as seen for the $N = 8$ case over one soliton period in **Figure 3**a.

© 2019 WILEY-VCH Verlag GmbH & Co. KGaA, Weinheim

For the dispersion parameters of our grating, soliton period is $z_0 = 17$ mm. From Figure 3a, we observe that in the absence of TOD, the pulse recovers its original shape at $z = z_0$. Turning on the TOD effects in our simulations breaks the spectral and temporal periodicity of soliton evolution as seen in Figure 3b, as the constituent fundamental solitons move at different speeds due to TOD. This results in the continuous separation of the breathers rather than the oscillations observed in Figure 3a and serves as an evidence that the onset of soliton fission is brought about by TOD in our grating. The soliton is not able to restore its initial spectral shape but instead, the separation in time manifests itself in the spectral domain as an overall broadening and formation of several spectral peaks, as well as a blueshift. Finally, we include loss and high-order dispersion and numerically solve Equation (2). The simulations in Figure 3c reveal that the initial input pulse evolves into separate pulse peaks. We may further conclude from the numerical simulations that gratings of uniform length $L_g \geq 4.8$ mm are sufficiently long for soliton dynamics and fission associated with a soliton order of $N = 8$ to be observed.

4. Time-Resolved Characterization of Soliton Compression and Fission

For time-resolved characterization, we used a FREG apparatus, shown in Figure S1, Supporting Information. FREG allows us to retrieve the exact temporal shape and the phase of the ultra-short pulses.[43] The FREG setup measures a set of time-gated spectra using the delayed input pulse and the output of CMBG. This provides us with the spectrograms which are used to extract the pulse intensity and phase via a numerical algorithm.[44] Further details on the measurement setup can be found in Supporting Information.

For the temporal and spectral observations of high-order soliton dynamics in CMBGs, picosecond Gaussian pulses are coupled into the gratings using tapered fibers. **Figure 4**a shows the intensity profile of the input pulses used in the experiments, generated by our source setup of cascaded mode-locked laser (MLL), waveshaper (WS), and Erbium-doped fiber amplifier (EDFA). We input these near-transform limited 4.93 ps pulses with approximately flat phase as shown in **Figure 5**a and observe the spectral and temporal evolution of the pulses as the power coupled into the gratings, and hence soliton order N, increases.

For $N = 2.2$ ($P_0 = 0.36$ W), the pulse compresses with a factor of $\times$ 1.8 as seen in Figure 4b with a slight broadening in the spectral domain. As we increase the input power further, the pulse gradually compresses up to a large soliton compression factor of $\times$ 5.7, exceeding the previous demonstrations of on-chip soliton-effect compression[8,9] for $N = 4.65$ ($P_0 = 1.62$ W), as shown in Figure 4c. Spectral broadening further increases and starts showing multiple peaks in both measurements and simulations. When we zoom into the phase at the center of the pulse in Figure 5c, the agreement between experiment and modeling becomes clearer; both are flat with an asymmetry induced by the grating's TOD.

We increased N by further increasing the coupled power into the grating and observed fission for the soliton order $N = 8.75$. Our simulations, as well as the measurements, show three clear peaks at an intensity exceeding a quarter of the peak intensity. Spectral characterization of the $N = 8.75$ ($P_0 = 5.73$ W) case reveals new spectral peaks on the blue side of the spectrum. It is expected from the nature of Fourier transformation that the temporal separation will be accompanied by spectral modulation. This is the same physical mechanism that initiates SC generation. The distinct peaks in the time domain show themselves as the new peaks forming in the frequency domain; a signature of the TOD-induced fission is the new peak formation in the anti-Stokes side.[39] This is seen in the spectral domain in Figure 4d at $\lambda = 1540$ nm for both modeling and experimental results. As a result of the pulse separation, we see phase differences between three consecutive pulses in our phase-resolved measurements, as seen in Figure 5d.

As the extent of spectral broadening is increased, the dispersion experienced by newly generated spectral fringes differs from that of the pulse's central wavelength. This results in the variations of widths and amplitudes of fundamental solitons in order to conserve their soliton order. Solitons that have undergone fission do not propagate as a single entity as the constituent fundamental solitons do not propagate with the same velocity. Considering the inherent uncertainties of high-power measurements and high order nonlinear effects, our modeling and time-resolved measurements, while not in perfect agreement, agree sufficiently well such that the underlying physics of soliton dynamics are well captured. Several factors can explain the moderate quantitative deviations; rapid change of dispersion at the band edge, divergences from the ideal input pulse shape, polarization tuning, power fluctuations as well as the complexity of modeling nonlinear effects induced by high input peak powers.

We observe through time-resolved measurements that the periodicity of soliton evolution breaks as the constituent fundamental solitons move at different speeds. This process, referred to as soliton fission, occurs here due to TOD perturbation.[21,39] Our modeling shown in Figures 3–5 constitutes further proof of fission in our cladding-modulated Bragg grating. In addition, analytic formalism from the literature states a threshold β_0, for TOD to break the symmetry of the propagating pulses and initiate the fission of high-order solitons. β_0 rapidly decreases with increasing N and the parameter β calculated as $\beta = \beta_3/6\beta_2 T_0$ should exceed the threshold β_0.[21] β also provides a means to control soliton interactions with TOD to improve bandwidth in fiber communications.[45] For conditions leading to $N = 3$, we are above the threshold value of β_0 required to initiate soliton fission as $\beta = 0.058$ for our CMBG.[21] Hence, we infer that we are also above this threshold for our experimental demonstration of soliton fission where $N = 8.75$ and conclude that the pulse splitting observed for $N = 8.75$ is a result of soliton fission occurring. Furthermore, the fission distance, which is defined by $L_{fiss} \approx L_{D2} / N$,[13] corresponds to $L_{fiss} = 1.23$ mm for the high power measurements ($N = 8.75$) which is much shorter than of our uniform grating length $L_g = 4.8$ mm. As N increases for higher power levels, the minimum grating length to observe fission would be even shorter at higher input peak powers.

5. Conclusion and Outlook

Nonlinear absorption occurring in silicon at the telecommunication wavelengths has hindered the realization of crucial

© 2019 WILEY-VCH Verlag GmbH & Co. KGaA, Weinheim

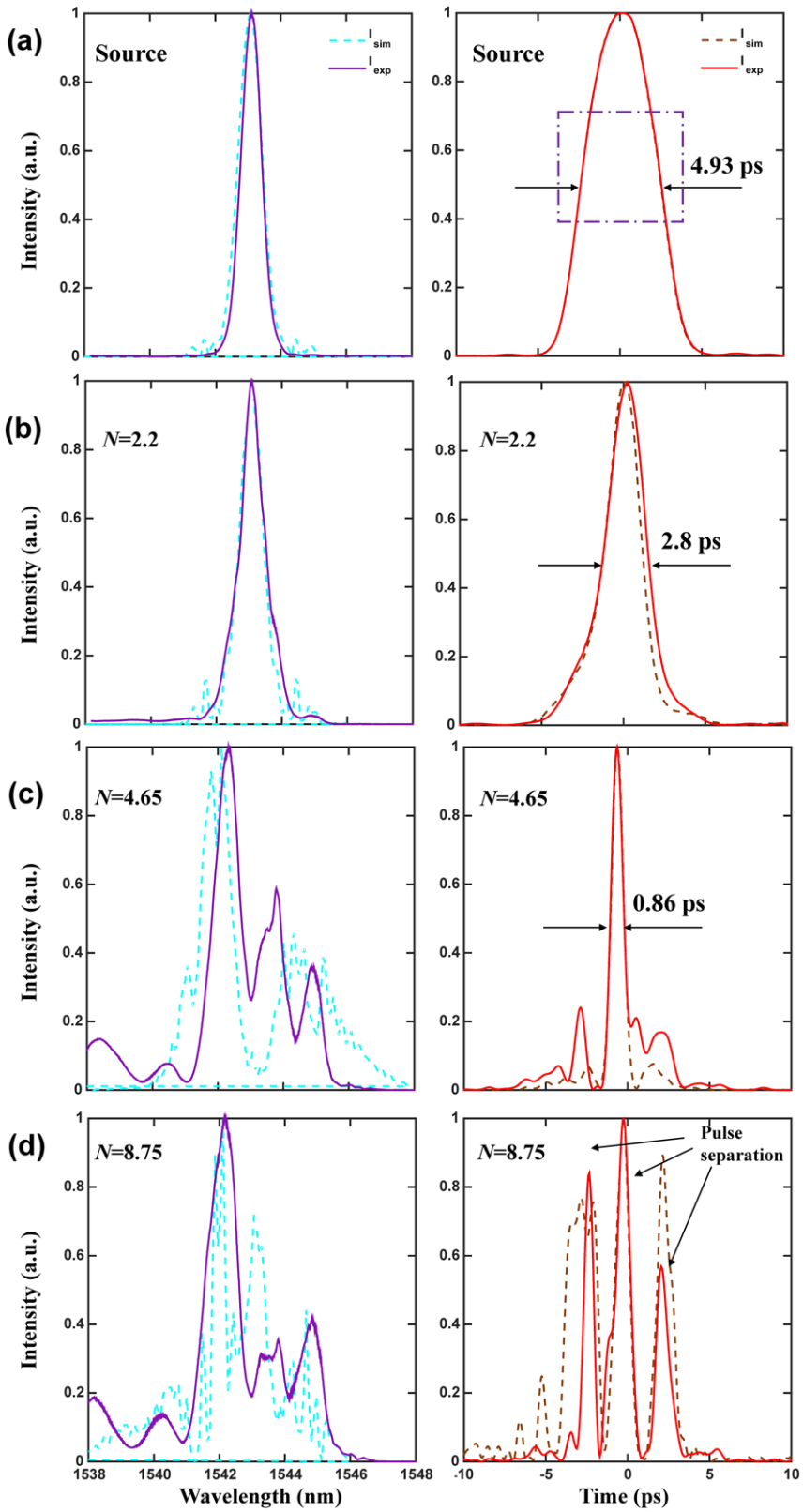

Figure 4. Temporal and spectral characterization of the pulses exiting the CMBG. Measured spectrum and temporal profile of: a) the source pulse, soliton evolution for: b) $N = 2.2$, c) $N = 4.65$, and d) $N = 8.75$ for $L_g = 4.8$ mm.

© 2019 WILEY-VCH Verlag GmbH & Co. KGaA, Weinheim

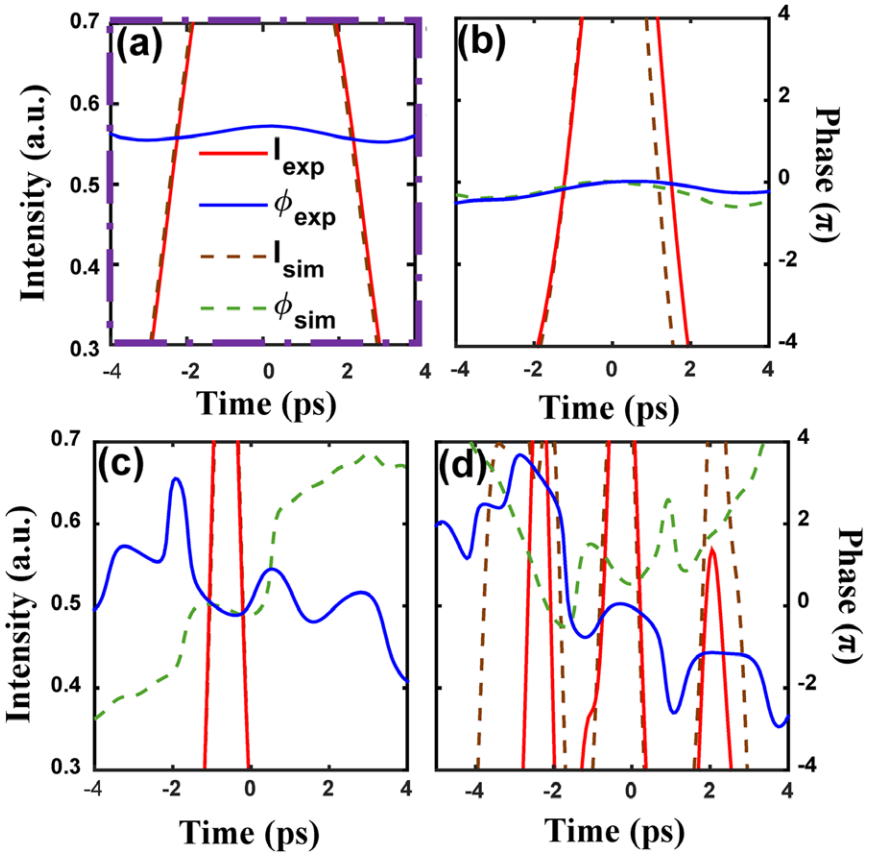

Figure 5. The measured phase at the pulse centers (as marked with purple dashed square in Figure 4a), from right to left; a) the source and high-order soliton evolution for: b) $N = 2.2$, c) $N = 4.65$, and d) $N = 8.75$ for $L_g = 4.8$ cm.

nonlinear effects such as soliton fission and strong soliton pulse compression. In this work, we overcome these issues by utilizing a novel CMOS-compatible material that is free of nonlinear absorption: ultra-silicon-rich nitride (USRN), in combination with cladding modulated integrated Bragg gratings. We harnessed Bragg soliton propagation to experimentally demonstrate the temporal profile of soliton fission on a CMOS-compatible chip, accompanied by a large soliton-effect picosecond pulse compression. We highlight the importance of our large high-order soliton compression result. Achieving a compression factor of **×** 5.7 through high-order soliton compression in CMOS-compatible platform is very promising for applications in optical signal processing and ultrafast integrated lasers; even larger compression factors can be achieved by exploiting higher soliton orders while using a shorter grating and larger powers that were not available in our current setup.

Soliton fission is one of the fundamental physical effects for initiating SC generation and it has been studied in this context in a variety of integrated platforms, including CMOS-compatible platforms.[13,14,46] Whereas these experiments provided valuable insight into soliton fission dynamics, they were constrained to the use of ultrashort femtosecond pulses and only spectral characterization was provided. Nevertheless, they revealed that nonlinear losses play a major role at inducing fission in nanowire waveguides, while free-carrier dispersion (FCD) is the dominant cause of fission in PhCWgs.[20] Interestingly, FCD plays a limiting role in pulse compression in PhCWgs.[9,47] We were able to characterize both large soliton compression and fission dynamics on the same device due to the combination of our grating structure and material platform which does not possess nonlinear losses. Soliton fission observed in our experiments is due to the large TOD brought about by the dispersion profile of the grating. TOD-induced soliton fission as an underlying phenomenon of SC generation in silicon wire waveguides was previously discussed[48] and require large soliton orders due to their dispersion profile, making it difficult to model and characterize the behavior of output pulses. The large soliton order and short pulse width (100 fs) indicate that they operate in a regime where nonlinear effects are more dominant whereas the dispersion profile of our grating enabled us to present the time-resolved characterization of the soliton fission using picosecond pulses.

On-chip soliton-based pulse compression has been demonstrated in 2D photonic crystal waveguides (PhCWgs); in non-CMOS-compatible GaInP (× 5.4 compression)[8] and silicon (× 2.3 compression).[9] The presence of two-photon absorption in silicon compromised the extent of soliton effect temporal compression to some degree,[9] and similarly limited the full soliton fission process. While PhCWgs have some similarities with Bragg gratings in that they enable much shorter length scales for soliton formation, Bragg gratings are fundamentally different

© 2019 WILEY-VCH Verlag GmbH & Co. KGaA, Weinheim

in how they guide light and are compatible with conventional waveguides, possess reduced propagation losses, and have mechanical robustness particularly compared to membrane-based PhCWgs. Another pulse compression scheme that involved a two-stage waveguide design on the silicon-on-insulator platform yielded record high result of 7 × compression.[49] This work used corrugated sidewall gratings as a dispersive element and compressed the pulse down to 1 ps FWHM via re-phasing using a separate nonlinear waveguide. Though useful for pulse compression, nonlinear and dispersive phases imparted on the input pulse are spatially separated, therefore it is inherently different to the soliton-based compression schemes described here and does not yield the soliton functionalities beyond pulse compression. Nonlinear pulse propagation in Bragg gratings, combined with the USRN platform which possesses a high nonlinear figure of merit,[36] may be effectively harnessed for novel functionalities with potential impact in various fields including ultrafast waveform metrology, imaging, and optical communications.

Furthermore, by carefully controlling the grating parameters, for example by introducing chirp,[35] high-repetition-rate soliton-trains can also be generated, as previously proposed for fiber Bragg gratings.[50] Using this method, the characteristics of the generated soliton-train, such as repetition rate and pulse width could also be tailored for advanced on-chip light sources at GHz repetition rates and with footprints significantly smaller than fiber-based systems. Our demonstration of soliton fission could herald a new class of on-chip light sources that leverage fission for femtosecond pulse train generation. Moreover, the fission process may be effectively leveraged for enhancing the efficiency of SC generation.[51] This work should inspire researchers to engineer and exploit higher-order dispersion in periodic media, to examine nonlinear pulse propagation, and in particular, to elucidate and harness the complex dynamics associated with pulse train generation and soliton fission.

Supporting Information

Supporting Information is available from the Wiley Online Library or from the author.

Acknowledgements

E.S. acknowledges scholarship funding Singapore International Graduate Award (SINGA) from A*STAR and thanks the Institute for Photonics and Optical Science (IPOS), the University of Sydney Nano Institute and the School of Physics at the University of Sydney for hosting her to conduct the experiments with A.B.R. D.T.H.T. acknowledges the support of the National Research Foundation Competitive Research Grant, MOE ACRF Tier 2 grant, SUTD – MIT International Design center, Digital Manufacturing and Design Grant and the National Research Foundation, Prime Minister's Office, Singapore, under its Medium Sized Centre Program. B.E. acknowledges the support of the Australian Research Council (ARC) Laureate Fellowship (FL120100029) and the Centre of Excellence program (CUDOS CE110001018).

Conflict of Interest

The authors declare no conflict of interest.

Keywords

Bragg gratings, Bragg soliton fission, integrated optics devices, nonlinear optics, optical solitons, silicon-rich nitride, ultrafast optics

Received: March 30, 2019
Revised: May 24, 2019
Published online:

[1] L. F. Mollenauer, R. H. Stolen, J. P. Gordon, *Phys. Rev. Lett.* **1980**, *45*, 1095.
[2] L. F. Mollenauer, J. P. Gordon, M. N. Islam, *IEEE J. Quantum Electron.* **1986**, *22*, 157.
[3] R. H. Stolen, W. J. Tomlinson, L. F. Mollenauer, *Opt. Lett.* **1983**, *8*, 186.
[4] I. M. Uzunov, V. D. Stoev, T. I. Tzoleva, *Opt. Lett.* **1992**, *17*, 1417.
[5] H. G. Winful, *Appl. Phys. Lett.* **1985**, *46*, 527.
[6] B. J. Eggleton, R. E. Slusher, C. M. de Sterke, P. A. Krug, J. E. Sipe, *Phys. Rev. Lett.* **1996**, *76*, 1627.
[7] P. Millar, R. M. De La Rue, T. F. Krauss, J. S. Aitchison, N. G. Broderick, D. J. Richardson, *Opt. Lett.* **1999**, *24*, 685.
[8] P. Colman, C. Husko, S. Combrié, I. Sagnes, C. W. Wong, A. De Rossi, *Nat. Photonics* **2010**, *4* 862.
[9] A. Blanco-Redondo, C. Husko, D. Eades, Y. Zhang, J. Li, T. F. Krauss, B. J. Eggleton, *Nat. Commun.* **2014**, *5*, 3160.
[10] J. T. Mok, I. C. M. Littler, E. Tsoy, B. J. Eggleton, *Opt. Lett.* **2005**, *30*, 2457.
[11] B. J. Eggleton, C. M. de Sterke, A. B. Aceves, J. E. Sipe, T. A. Strasser, R. E. Slusher, *Opt. Commun.* **1998**, *149*, 267.
[12] Q. Li, K. Nakkeeran, P. K. A. Wai, *J. Opt. Soc. Am. B* **2014**, *31*, 1786.
[13] J. M. Dudley, G. Genty, S. Coen, *Rev. Mod. Phys.* **2006**, *78*, 1135.
[14] F. Leo, J. Safioui, B. Kuyken, G. Roelkens, S.-P. Gorza, *Opt. Express* **2014**, *22*, 28997.
[15] R. K. W. Lau, M. R. E. Lamont, A. G. Griffith, Y. Okawachi, M. Lipson, A. L. Gaeta, *Opt. Lett.* **2014**, *39*, 4518.
[16] T. Wang, D. K. T. Ng, S. K. Ng, Y. T. Toh, A. K. L. Chee, G. F. R. Chen, Q. Wang, D. T. H. Tan, *Laser Photonics Rev.* **2015**, *9*, 498.
[17] M. Yu, J. K. Jang, Y. Okawachi, A. G. Griffith, K. Luke, S. A. Miller, X. Ji, M. Lipson, A. L. Gaeta, *Nat. Commun.* **2017**, *8*, 14569.
[18] T. J. Kippenberg, A. L. Gaeta, M. Lipson, M. L. Gotodetsky, *Science* **2018**, *361*, eaan8083.
[19] C. Husko, M. Wulf, S. Lefrancois, S. Combrié, G. Lehoucq, A. De Rossi, B. J. Eggleton, L. Kuipers, *Nat. Commun.* **2016**, *7*, 11332.
[20] C. Ciret, S.-P. Gorza, C. Husko, G. Roelkens, B. Kuyken, F. Leo, *Sci. Rep.* **2018**, *8*, 17177.
[21] P. K. A. Wai, C. R. Menyuk, Y. C. Lee, H. H. Chen, *Opt. Lett.* **1986**, *11*, 464.
[22] W. Chen, D. L. Mills, *Phys. Rev. Lett.* **1987**, *58*, 160.
[23] C. M. de Sterke, J. E. Sipe, *Phys. Rev. A* **1989**, *39*, 5163.
[24] J. T. Mok, C. M. de Sterke, I. C. M. Littler, B. J. Eggleton, *Nat. Phys.* **2006**, *2*, 775.
[25] A. B. Aceves, S. Wabnitz, *Phys. Lett. A* **1989**, *141*, 37.
[26] D. N. Christodoulides, R. I. Joseph, *Phys. Rev. Lett.* **1989**, *62*, 1746.
[27] J. E. Sipe, H. G. Winful, *Opt. Lett.* **1988**, *13*, 132.
[28] G. Coppola, A. Irace, A. Cutolo, M. Iodice, *Appl. Opt.* **1999**, *38*, 1752.
[29] A. D. Simard, N. Ayotte, Y. Painchaud, S. Bédard, S. LaRochelle, *J. Lightwave Technol.* **2011**, *29*, 3693.
[30] A. D. Simard, G. Beaudin, V. Aimez, Y. Painchaud, S. LaRochelle, *Opt. Express* **2013**, *21*, 23145.
[31] G. Jiang, R. Chen, Q. Zhou, J. Yang, M. Wang, X. Jiang, *IEEE Photonics Technol. Lett.* **2010**, *23*, 6.
[32] X. Wang, Y. Wang, J. Flueckiger, R. Bojko, A. Liu, A. Reid, J. Pond, N. A. F. Jaeger, L. Chrostowski, *Opt. Lett.* **2014**, *39*, 5519.

© 2019 WILEY-VCH Verlag GmbH & Co. KGaA, Weinheim

[33] B. Naghdi, L. R. Chen, *Opt. Express* **2016**, *24*, 23429.
[34] D. T. H. Tan, K. Ikeda, Y. Fainman, *Opt. Lett.* **2009**, *34*, 1357.
[35] E. Sahin, K. J. A. Ooi, C. E. Png, D. T. H. Tan, *Appl. Phys. Lett.* **2017**, *110*, 161113.
[36] K. J. A. Ooi, D. K. T. Ng, T. Wang, A. K. L. Chee, S. K. Ng, Q. Wang, L. K. Ang, A. M. Agarwal, L. C. Kimerling, D. T. H. Tan, *Nat. Commun.* **2017**, *8*, 13878.
[37] E. Dulkeith, Y. A. Vlasov, X. Chen, N. C. Panoiu, R. M. Osgood, Jr., *Opt. Express* **2006**, *14*, 5524.
[38] L. Yin, G. P. Agrawal, *Opt. Lett.* **2007**, *32*, 2031.
[39] G. P. Agrawal, *Nonlinear Fiber Optics*, Elsevier Science, Amsterdam, The Netherlands **2013**.
[40] B. J. Eggleton, C. M. de Sterke, R. E. Slusher, *J. Opt. Soc. Am. B* **1999**, *16*, 587.
[41] C. M. de Sterke, J. E. Sipe, *Prog. Opt.* **1994**, *33*, 203.
[42] *Nonlinear Photonic Crystals* (Eds: R. E. Slusher, B. J. Eggleton), Springer, Berlin, Germany **2003**.
[43] C. Dorrer, I. Kang, *Opt. Lett.* **2002**, *27*, 1315.
[44] B. C. Thomsen, M. A. F. Roelens, R. T. Watts, D. J. Richardson, *IEEE Photonics Technol. Lett.* **2005**, *17*, 1914.
[45] P. L. Chu, C. Desem, *Electron. Lett.* **1985**, *21*, 228.
[46] L. Yin, Q. Lin, G. P. Agrawal, *Opt. Lett.* **2007**, *32*, 391.
[47] A. Blanco-Redondo, D. Eades, J. Li, S. Lefrancois, T. F. Krauss, B. J. Eggleton, C. Husko, *Optica* **2014**, *1*, 299.
[48] I.-W. Hsieh, X. Chen, X. Liu, J. I. Dadap, N. C. Panoiu, C.-Y. Chou, F. Xia, W. M. Green, Y. A. Vlasov, R. M. Osgood, Jr., *Opt. Express* **2007**, *15*, 15242.
[49] D. T. H. Tan, P. C. Sun, Y. Fainman, *Nat. Commun.* **2010**, *1*, 116.
[50] N. M. Litchinitser, G. P. Agrawal, B. J. Eggleton, G. Lenz, *Opt. Express* **1998**, *3*, 411.
[51] J. N. Kutz, C. Lyngå, B. J. Eggleton, *Opt. Express* **2005**, *13*, 3989.

© 2019 WILEY-VCH Verlag GmbH & Co. KGaA, Weinheim